

Detectability of Black Hole Binaries with *Gaia*: Dependence on Binary Evolution Models

MINORI SHIKAUCHI,^{1,2} ATARU TANIKAWA,³ AND NORITA KAWANAKA^{4,5,6}

¹*Department of Physics, the University of Tokyo, 7-3-1 Hongo, Bunkyo, Tokyo 113-0033, Japan*

²*Research Center for the Early Universe (RESCEU), the University of Tokyo, 7-3-1 Hongo, Bunkyo, Tokyo 113-0033, Japan*

³*Department of Earth Science and Astronomy, College of Arts and Sciences, the University of Tokyo, 3-8-1 Komaba, Meguro, Tokyo 153-8902, Japan*

⁴*Department of Astronomy, Graduate School of Science, Kyoto University, Kitashirakawa Oiwake-cho, Sakyo-ku, Kyoto, 606-8502, Japan*

⁵*Hakubi Center, Kyoto University, Yoshida-honmachi, Sakyo-ku, Kyoto, 606-8501, Japan*

⁶*Yukawa Institute for Theoretical Physics, Kyoto University, Kitashirakawa Oiwake-cho, Sakyo-ku, Kyoto, 606-8502, Japan*

(Received December 9, 2021; Revised February 4, 2022; Accepted February 7, 2022)

ABSTRACT

Astrometric satellite *Gaia* is expected to observe non-interacting black hole (BH) binaries with luminous companions (LCs) (hereafter BH-LC binaries), a different population from BH X-ray binaries previously discovered. The detectability of BH-LC binaries with *Gaia* might be dependent on binary evolution models. We investigated the *Gaia*'s detectability of BH-LC binaries formed through isolated binary evolution by means of binary population synthesis technique, and examined its dependence on single and binary star models: supernova models, common envelope (CE) ejection efficiency α , and BH natal kick models. We estimated that 1.1 – 46 BH-LC binaries can be detected within five-year observation, and found that α has the largest impacts on the detectable number. In each model, observable and intrinsic BH-LC binaries have similar distributions. Therefore, we found three important implications: (1) if the lower BH mass gap is not intrinsic (*i.e.* 3 – 5 M_{\odot} BHs exist), *Gaia* will observe $\leq 5M_{\odot}$ BHs, (2) we may observe short orbital period binaries with light LCs if CE efficiency is significantly high, and (3) we may be able to identify the existence of natal kick from eccentricity distribution.

Keywords: astrometry — stars: black holes — binaries: general

1. INTRODUCTION

Stellar mass black holes (BHs) are formed at the end of massive stars. Some previous researches estimated that there are $10^8 - 10^9$ stellar mass BHs in the Milky Way (MW) (Shapiro & Teukolsky 1983; van den Heuvel 1992; Brown & Bethe 1994; Samland 1998; Agol et al. 2002). Some of them have been detected as X-ray binaries in the MW and they have very short periods such as several hours. Less than 100 (Corral-Santana et al. 2016) BHs were detected in this way, much less than theoretically predicted.

Gravitational wave (GW) observation is an alternative way to find binaries including BHs. In extragalactic distances, more than 60 binary BHs/ neutron star(NS)-BH binaries have been detected (Abbott et al. 2019; The LIGO Scientific Collaboration et al. 2021). Thus, BH searches so far discovered BHs in short period binaries, which have electromagnetic and/or GW emissions through interactions between BHs and their companions.

There are two other ways to search for binaries consisting of BHs and luminous companions (LCs) (hereafter, BH-LC binaries) with longer orbital periods: radial velocity observations and astrometric observations. There are already a few detection reports of long orbital period BH-LC binaries with radial velocity search (Giesers et al. 2018; Thompson et al. 2019; Liu et al. 2019). In particular, Liu et al. (2019) have reported a $70M_{\odot}$ BH in a binary system (but see

Eldridge et al. 2020; Tanikawa et al. 2020; Safarzadeh et al. 2019; El-Badry & Quataert 2020; Irrgang et al. 2020). Thompson et al. (2019) found a non-interacting giant star-unseen object binary by combining radial velocity and photometric data. Since the mass of unseen object is estimated to be $3.3_{-0.7}^{+2.8} M_{\odot}$, it should be a light BH or massive NS, although the result is under debate (van den Heuvel & Tauris 2020; Thompson et al. 2020). Also, by employing radial velocity and photometric data, Jayasinghe et al. (2021) reported a binary consisting of a red giant V723 Mon and a BH candidate with its mass of $3.04 \pm 0.06 M_{\odot}$. In astrometric observations, Gould & Salim (2002) investigated BHs not producing supernovae (SNe) for the first time by using data sets of Hipparcos and indicated that the successor will observe their companion stars. As the successor of *Hipparcos*, *Gaia* mission (Gaia Collaboration et al. 2016) was launched in 2013 and has been providing information about parallaxes and proper motions of 2000 million stars with higher precision such as μas ¹. Now, *Gaia* Early Data Release 3 (EDR3) has been released², and the next data release (DR3) including full information of binaries, is planned in 2022³. Since the cadence of the observation is about 50 days and *Gaia* has been in science mode for several years, DR3 may include BH-LC binaries with longer periods than those that can be detected in X-rays or GWs, whose typical periods are hours to years. Moreover, it can observe a dark compact objects such as a NS, a white dwarf and a brown dwarf and LC binaries with a good precision (Andrews et al. 2019).

Some previous researches have estimated hundreds to thousands of BH-LC binaries can be detected with *Gaia* (Mashian & Loeb 2017; Breivik et al. 2017; Yamaguchi et al. 2018; Yalinewich et al. 2018; Kinugawa & Yamaguchi 2018; Shao & Li 2019; Chawla et al. 2021). All of the binaries so far were thought to be isolated binaries, which were born as tight binaries and did not experience any dynamical interactions with other stars in the MW disk. In stellar clusters, BH-LC binaries can be formed by dynamical interactions and Shikauchi et al. (2020) estimated about 10 BH-main sequence (MS) star binaries can be detected. The detectability is greatly affected by binary evolution models and observational constraints they employed. However, the previous researches investigated how the detectability will be affected by one or two of the binary evolution models: SN models, common envelope (CE) efficiency α , and natal kick models. In this work, we employ binary population synthesis to see how all the combinations of the binary evolution models affect the detectability, and discuss whether we can give constraints on binary evolution models from current/future observations with stringent observational constraints employed in Yamaguchi et al. (2018).

The structure of this paper is as follows. In section 2, we introduce the binary evolution models used in this work, and we summarize the observational constraints. We show the results of binary population synthesis in section 3 and discuss the difference among our results and previous works in section 4.

2. METHOD

In this section, we first summarize a initial setup for the simulation: the spatial distribution of BH-LC binaries and initial conditions of binaries in subsection 2.1. We also introduce a binary population synthesis code and modifications that we added to it in subsection 2.2. Then We summarize how to obtain the number of detectable BH-LC binaries with *Gaia* in subsection 2.3. It is based on Yamaguchi et al. (2018).

2.1. Initial Condition

On the assumption that we get the same BH-LC population everywhere in the MW disk, the number of binaries at a position, \mathbf{x} , can be expressed as a function of their BH masses, m_{BH} , LC masses, m_{LC} , orbital periods, P , and eccentricities e ,

$$N(m_{\text{BH}}, m_{\text{LC}}, P, e, \mathbf{x}) = \tilde{N}(m_{\text{BH}}, m_{\text{LC}}, P, e) \times t_{\text{LC}} \times \dot{\rho}(\mathbf{x}), \quad (1)$$

where $\tilde{N}(m_{\text{BH}}, m_{\text{LC}}, P)$ is

$$\tilde{N}(m_{\text{BH}}, m_{\text{LC}}, P, e) = N_{\text{sim}}(m_{\text{BH}}, m_{\text{LC}}, P, e) / M_{\text{ini,int}}, \quad (2)$$

where $N_{\text{sim}}(m_{\text{BH}}, m_{\text{LC}}, P, e)$ is the number of binaries with m_{BH} , m_{LC} , P , and e in our simulations, t_{LC} is the lifetime of LC, $\dot{\rho}(\mathbf{x})$ is a formation rate density of stars in the MW ($M_{\odot}\text{pc}^{-3}\text{year}^{-1}$), and $M_{\text{ini,int}}$ is the intrinsic total mass of binaries in one realization. Note that the value $M_{\text{ini,int}}$ is not equal to the total initial mass in our simulation, $M_{\text{ini,sim}}$: we simulate the evolution of binaries whose minimum primary mass is $8M_{\odot}$, while the actual minimum primary mass

¹ <https://www.cosmos.esa.int/web/gaia/science-performance>

² <https://www.cosmos.esa.int/web/gaia/earlydr3>

³ <https://www.cosmos.esa.int/web/gaia/release>

should be as small as $0.08M_{\odot}$, so the initial total mass of binaries in our simulation is smaller than that in reality. Considering that $M_{\text{ini,sim}}$ is $3.1 \times 10^7 M_{\odot}$, we adopt $M_{\text{ini,int}} = 1.5 \times 10^8 M_{\odot}$.

In this work, we consider only the MW disk because the interstellar extinction makes it difficult to observe the binaries in the bulge. We assume that a local star-formation rate density is proportional to a local stellar density, and that star formation rate, R_{SF} , is constant everywhere in the MW disk. We adopt a total star formation rate in the entire MW disk to R_{SF} , $3.5M_{\odot} \text{ year}^{-1}$ (O’Shaughnessy et al. 2008). Then, a formation rate density $\dot{\rho}(\mathbf{x})$ is given by

$$\dot{\rho}(\mathbf{x}) = R_{\text{SF}} \times n_{\text{MW}}(\mathbf{x}), \quad (3)$$

where $n_{\text{MW}}(\mathbf{x})$ is a stellar number density distribution at a position \mathbf{x} in the MW. In the MW disk, we assume that stars are exponentially distributed from the center of the galaxy (de Vaucouleurs 1959; Kormendy 1977) and perpendicular to the galaxy plane (Bahcall & Soneira 1980). The stellar number density distribution $n_{\text{MW}}(\mathbf{x})$ can then be expressed as

$$n_{\text{MW}}(\mathbf{x}(r, z)) = n_0 \exp\left(-\frac{r-r_0}{r_h} - \frac{z}{h_z}\right), \quad (4)$$

where $r_0 = 8.5$ kpc is the distance from the center of the Galaxy to the sun, and $r_h = 3.5$ kpc and $h_z = 250$ pc are the scale lengths along the r - and z - directions, respectively. We adopt the normalization factor, n_0 , to satisfy the following equation,

$$4\pi \int_0^{r_{\text{max}}} r dr \int_0^{z_{\text{max}}} dz n_{\text{MW}}(\mathbf{x}) = 1, \quad (5)$$

and we set $r_{\text{max}} = 30$ kpc and $z_{\text{max}} = 1$ kpc (see a review for Bland-Hawthorn & Gerhard 2016).

SN model	α	kick	N_{det}	$N_{\text{det}}(P > 1 \text{ year})$	SN model	α	kick	N_{det}	$N_{\text{det}}(P > 1 \text{ year})$
rapid	0.1	no kick	27	26	delayed	0.1	no kick	15	14
...	1.0	...	28	28	...	1.0	...	22	20
...	10	...	40	33	...	10	...	46	36
...	0.1	FB kick	17	17	...	0.1	FB kick	1.5	0.82
...	1.0	...	18	18	...	1.0	...	1.1	0.85
...	10	...	31	24	...	10	...	9.4	2.4

Table 1. The detectability of BH-LC binaries with *Gaia* with different models. The mark “...” represents a repeat of the same model above. We estimated 1.1–46 binaries can be detected. The value $N_{\text{det}}(P > 1 \text{ year})$ indicates the detectability of BH-LC binaries with period longer than 1 year.

Our initial conditions are following. We employ Kroupa initial mass function (Kroupa 2001) as the initial mass function of the primary mass. The minimum and maximum masses are set to be $8M_{\odot}$ and $150M_{\odot}$, respectively. We assume a flat mass ratio distribution from 0 to 1 (Kuiper 1935; Kobulnicky & Fryer 2007) and obtain the secondary mass. We set the minimum value of the secondary mass to $0.1M_{\odot}$. For the distribution of initial semi-major axis, we assume a logarithmically flat distribution from $10R_{\odot}$ to 10^6R_{\odot} . The initial eccentricity is set to be thermally distributed (Heggie 1975). We employ the solar metallicity, $Z = 0.02$ to the metallicity.

2.2. Binary Population Synthesis Code and Modifications

In order to simulate the potential population of BH-LC binaries, we employ binary population synthesis code BSE (Hurley et al. 2000; Hurley et al. 2002). Stellar wind models are updated to metallicity-dependent ones following Belczynski et al. (2010). Using BSE, we simulate the evolution of millions of binaries. They start from zero-age MS binary stars and some physical processes such as mass and angular momentum transfers, CE phases, BH formations and natal kicks.

Here, we adopt some modifications as follows. First, we employ SN models suggested in Fryer et al. (2012). There are two models: “the rapid model” and “the delayed model”. In the former model, only very few compact remnants whose mass is in the range of $2 - 4.5M_{\odot}$ are formed. The resulting gap in the compact remnant mass function matches the observations (Özel et al. 2010; Farr et al. 2011). On the other hand, the latter model does not produce such a mass gap. Indeed, whether the observed BH mass gap is intrinsic or not is still controversial. Therefore, we employ these two

models to see how they affect both the detectability and binary parameter distributions such as BH and LC masses. Second, we employ different CE efficiencies α . When the mass transfer is dynamically unstable during Roche Lobe overflow (RLOF), a binary will enter CE phase. We use an energy conservation equation derived in [Webbink \(1984\)](#) to treat CE evolution. One of the CE parameters λ includes an effect of the mass distribution within the envelope and a contribution from the internal energy ([de Kool 1990](#); [Dewi & Tauris 2000](#)). We employ the results in [Claeys et al. \(2014\)](#) to obtain λ . Also, the other parameter α is CE efficiency with which the orbital energy is used to eject the mass donor’s envelope. Since the value of α is of great uncertainty ([Fragos et al. 2019](#); [Podsiadlowski et al. 2003](#); [Kiel & Hurley 2006](#); [Yungelson & Lasota 2008](#); [Mapelli & Giacobbo 2018](#); [Chu et al. 2022](#); [Broekgaarden & Berger 2021](#)), we adopt a variety of CE efficiencies, $\alpha = 1$, $\alpha = 0.1$, and $\alpha = 10$. Finally, for BH natal kick, we consider two cases: no kick and “fallback (FB) kick”. For FB kick, we reduce a NS natal kick by a factor of $(1 - f_{\text{fb}})$, where f_{fb} is a fraction of mass of fallback matter to all the ejected mass during SN explosion. NS kick follows Maxwellian distribution with $\sigma = 265 \text{ km s}^{-1}$ ([Hobbs et al. 2005](#)).

In summary, we treat 12 parameter sets with different two SN models, three values of α , and two natal kick models. For each parameter set, we simulated 10^6 binary stars. In the following sections, we refer each binary evolution model set as “SN model/the value of CE efficiency/kick model”. For example, “rapid/ $\alpha = 1$ /no kick model” indicates the rapid model with CE efficiency $\alpha = 1$ and no natal kick.

2.3. Number Estimation

In the following, we summarize how we assume the distribution of binaries obtained in BSE simulations in the MW (2.1), and the observational constraints for *Gaia* (2.3.1, 2.3.2) following [Yamaguchi et al. \(2018\)](#).

Based on the spatial distribution of the binaries in the MW, we calculate the total number of BH-LC binaries detectable with *Gaia*, N_{det} , by summing up $n(m_{\text{BH}}, m_{\text{LC}}, P, e, \mathbf{x})$ over m_{BH} , m_{LC} , P , e , and a distance to the binary D up to the maximum distance D_{max} ,

$$N_{\text{det}} = \int dm_{\text{BH}} \int dm_{\text{LC}} \int dP \int de \int_{|\mathbf{x}-\mathbf{x}_0| < D_{\text{max}}} d^3\mathbf{x} N(m_{\text{BH}}, m_{\text{LC}}, P, e, \mathbf{x}), \quad (6)$$

where \mathbf{x}_0 is the position of the Sun.

Note that D_{max} is dependent on the parameters of the binaries such as m_{BH} , m_{LC} and orbital separation a . In the following section, we obtain three constraints on D_{max} : D_{LC} obtained considering interstellar extinction, D_{II} and D_a for the confident detection of BHs (see below equation 17 and 18 respectively). Therefore, we set $D_{\text{max}} = \min(D_{\text{LC}}, D_{\text{II}}, D_a)$. In the following sections, we introduce how to evaluate D_{LC} , D_{II} and D_a .

2.3.1. Interstellar Extinction

Here, we evaluate the maximum distance at which the LC of a binary is so luminous that it can be observed with *Gaia*, D_{LC} . We consider interstellar extinction and D_{LC} is dependent on a luminosity of LC, L_{LC} , and an effective temperature, $T_{\text{eff,LC}}$, satisfying the equation below,

$$m_{\text{V}}(L_{\text{LC}}, T_{\text{eff,LC}}, D_{\text{LC}}) = m_{\text{v,lim}}, \quad (7)$$

where $m_{\text{v,lim}}$ is the maximum apparent magnitude with which a binary can be observed with *Gaia*. We set $m_{\text{v,lim}} = 20$ ([Gaia Collaboration et al. 2016](#)). By following [Yamaguchi et al. \(2018\)](#), we consider V band instead of the *Gaia* band because the color $V - I$ can be less than unity (see Figure 14 of [Jordi et al. 2010](#)). The V-band absolute magnitude of a LC, M_{V} , can be obtained from L_{LC} and $T_{\text{eff,LC}}$ taking into account the bolometric correction (see equation 1, 10, and Table 1 in [Torres 2010](#)).

The apparent magnitude, m_{V} , can be obtained by using the relationship shown below,

$$M_{\text{V}}(L_{\text{LC}}, T_{\text{eff,LC}}) = m_{\text{v}} - 5(2 + \log_{10} D/\text{kpc}) - A_{\text{V}}(D/\text{kpc}), \quad (8)$$

where D is the distance to the binary and A_{V} is a term of interstellar extinction. Considering the average extinction in the MW is $\sim 1 \text{ mag per 1 kpc}$ in V band ([Spitzer 1978](#); [Shafter 2017](#)), we assume $A_{\text{V}} \sim D/\text{kpc}$. Then, we obtain D_{LC} satisfying the following equation,

$$M_{\text{V}}(L_{\text{LC}}, T_{\text{eff,LC}}) + 5(2 + \log_{10} D_{\text{LC}}/\text{kpc}) + D_{\text{LC}}/\text{kpc} = m_{\text{v,lim}}. \quad (9)$$

2.3.2. Observational Constraints on Confirmed Detection of BHs

Through astrometric observations, we can identify a LC with a sinusoidal motion as a part of binary consisting of the visible LC and an unseen object. To determine the unseen object as a BH, we set the lower limit of the unseen object mass should be larger than $2M_\odot$, that is, the estimated mass of the unseen object should satisfy the equation below

$$m_{\text{BH}} - n\sigma_{\text{BH}} > 2M_\odot, \quad (10)$$

where m_{BH} is the unseen object mass and σ_{BH} is its standard error. We set $n = 1$ following Yamaguchi et al. (2018). There is a caveat: NSs might be contaminated under the condition we use here. However, in GW190814 (Abbott et al. 2020), a compact object with $2 - 3M_\odot$ was detected and it is worth searching for objects within such mass range even if they are not BHs.

The observables of a binary are the LC mass, m_{LC} , the orbital period, P , the angular semi-major axis, a_* , and a distance to the binary, D . They can be expressed in one equation shown below,

$$\frac{(m_{\text{LC}} + m_{\text{BH}})^2}{m_{\text{BH}}^3} = \frac{G}{4\pi^2} \frac{P^2}{(a_*D)^3}, \quad (11)$$

where G is a gravitational constant. Using equation (11), we relate the standard error of BH mass, σ_{BH} , to standard errors of other binary parameters,

$$\left(\frac{\sigma_{\text{BH}}}{m_{\text{BH}}}\right)^2 = \left(\frac{3}{2} - \frac{m_{\text{BH}}}{m_{\text{BH}} + m_{\text{LC}}}\right)^{-2} \left[\left(\frac{m_{\text{LC}}}{m_{\text{BH}} + m_{\text{LC}}}\right)^2 \frac{\sigma_{\text{LC}}^2}{m_{\text{LC}}^2} + \frac{\sigma_P^2}{P^2} + \frac{9}{4} \left(\frac{\sigma_{a_*}^2}{a_*^2} + \frac{\sigma_D^2}{D^2}\right) \right]. \quad (12)$$

where σ_{LC} , σ_{a_*} , σ_P , and σ_D are observational errors of the LC mass, the semi-major axis, the orbital period, and the distance of the binary, respectively. We assume that observational errors are sufficiently smaller than each observable, and we also ignore the correlation among the observables.

In order to confirm a detection, when we assume that each standard error should be smaller than 10% of the value of each variable, that is,

$$\frac{\sigma_{\text{LC}}}{m_{\text{LC}}} < 0.1, \quad \frac{\sigma_P}{P} < 0.1, \quad \frac{\sigma_{a_*}}{a_*} < 0.1, \quad \text{and} \quad \frac{\sigma_D}{D} < 0.1, \quad (13)$$

BHs with masses of $\gtrsim 3.4M_\odot$ will be confirmed to be detected.

Tetzlaff et al. (2011) indicated that a typical standard error of a stellar mass estimated from its spectral and luminosity is smaller than 10 %. Therefore, the first condition in equation (13) can be easily achieved. A standard error of an orbital period can be suppressed to $\lesssim 10\%$ when the observed period is shorter than two-thirds of the observational time (ESA 1997). Recently Lucy (2014) indicated we may be able to recover binary parameters even when the coverage of orbital period is as low as 40 % and O'Neil et al. (2019) proposed a new method to estimate binary parameters when the coverage is less than 40 %. Since *Gaia* has been observing for five years, we adopt 10 years to the maximum period. For the minimum period, we adopt 50 day, the cadence of *Gaia*, to it following Yamaguchi et al. (2018).

From the rest conditions, two more constraints can be imposed on D_{max} . Since a parallax Π is inversely proportional to the distance to a binary, we obtain the following equation,

$$\frac{\sigma_\Pi}{\Pi} \sim \frac{\sigma_D}{D} < 0.1, \quad (14)$$

where σ_Π is a standard error of a parallax. Based on Gaia Collaboration et al. (2016), σ_Π in G band can be expressed by the apparent magnitude m_v ,

$$\sigma_\Pi = (-1.631 + 680.8z(m_v) + 32.73z(m_v)^2)^{1/2} [\mu\text{as}], \quad (15)$$

where

$$z(m_v) = 10^{0.4(\max[12.09, m_v] - 15)}. \quad (16)$$

Here, we neglect the dependence on the color ($V - I$). Substituting equation (15) into equation (14), we obtain the constraint on D as

$$\left(\frac{D}{\text{kpc}}\right) < D_\Pi = \frac{10^2}{(-1.631 + 680.8z(m_v) + 32.73z(m_v)^2)^{1/2}}. \quad (17)$$

With respect to the constraint on a standard error of a semi-major axis, we obtain the other constraint on D_{\max} . Considering the semi-major axis of each binary is about the orbital radius on the celestial sphere, the standard error of semi-major axis, σ_{a^*} , is $\sim \sigma_{\Pi}$. The constraint derived from the condition of a semi-major axis can be expressed as

$$\left(\frac{D}{\text{kpc}}\right) < D_a = \frac{am_{\text{BH}}}{10(m_{\text{BH}} + m_{\text{LC}})\sigma_{\Pi}}. \quad (18)$$

Therefore, by adopting the minimum value among D_{LC} , D_{II} , and D_a as D_{\max} , we consider all the constraints for confident detection of BHs with *Gaia*. We also set the maximum distance as 10 kpc without considering any constraints as Yamaguchi et al. (2018) did.

3. RESULT

The detectabilities N_{det} with different binary evolution models are shown in Table 1. We found that 1.1 – 46 BH-LC binaries can be detected. We also show the detectability of binaries with orbital period longer than 1 year, $N_{\text{det}}(P > 1 \text{ year})$. For most of the models, long period binaries are dominant in the detectable ones.

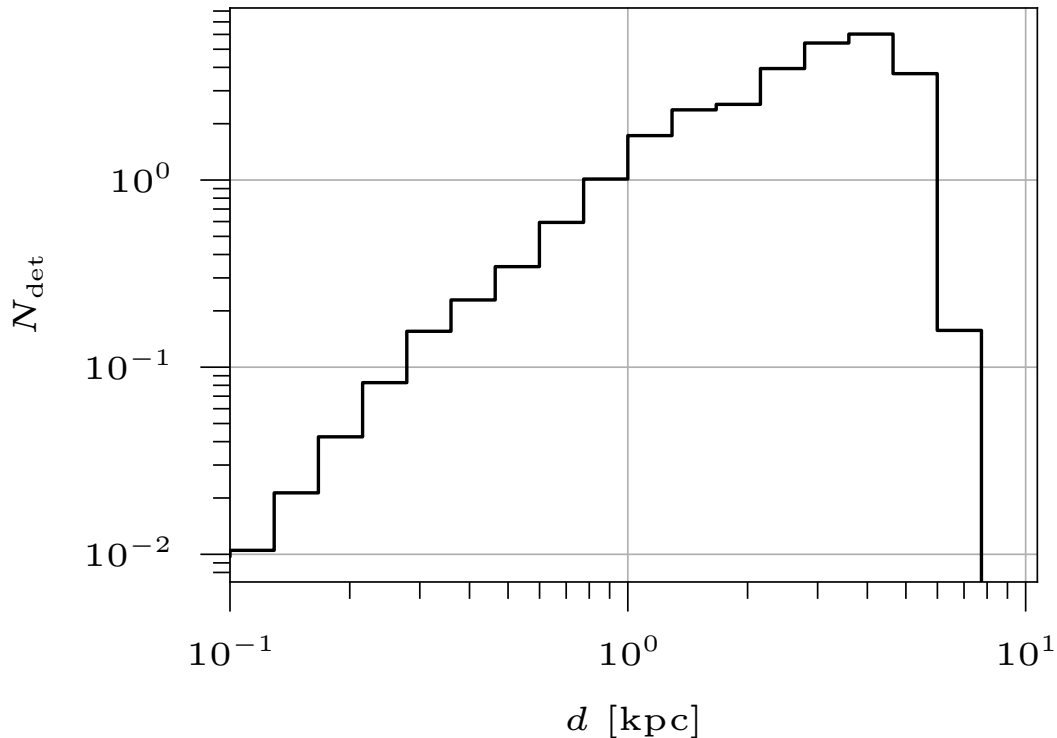


Figure 1. The number of detectable BH-LC binaries N_{det} in rapid/ $\alpha = 1$ /no kick model as a function of a distance to them from the Sun, d [kpc].

Figure 1 shows the number of detectable BH-LC binaries N_{det} in rapid/ $\alpha = 1$ /no kick model with respect to a distance to them from the Sun, d [kpc]. The number of detectable binaries monotonically increases as the integrated volume does. However, around $d = 4$ kpc the detectability drastically decreases because the observational constraints on the orbital separations are so stringent that farther binaries cannot be detected.

3.1. Predictions of Detectable Binary Parameter Distributions

Here, we investigate how binary evolution models affect binary parameter distributions and discuss whether we can identify them from the observation.

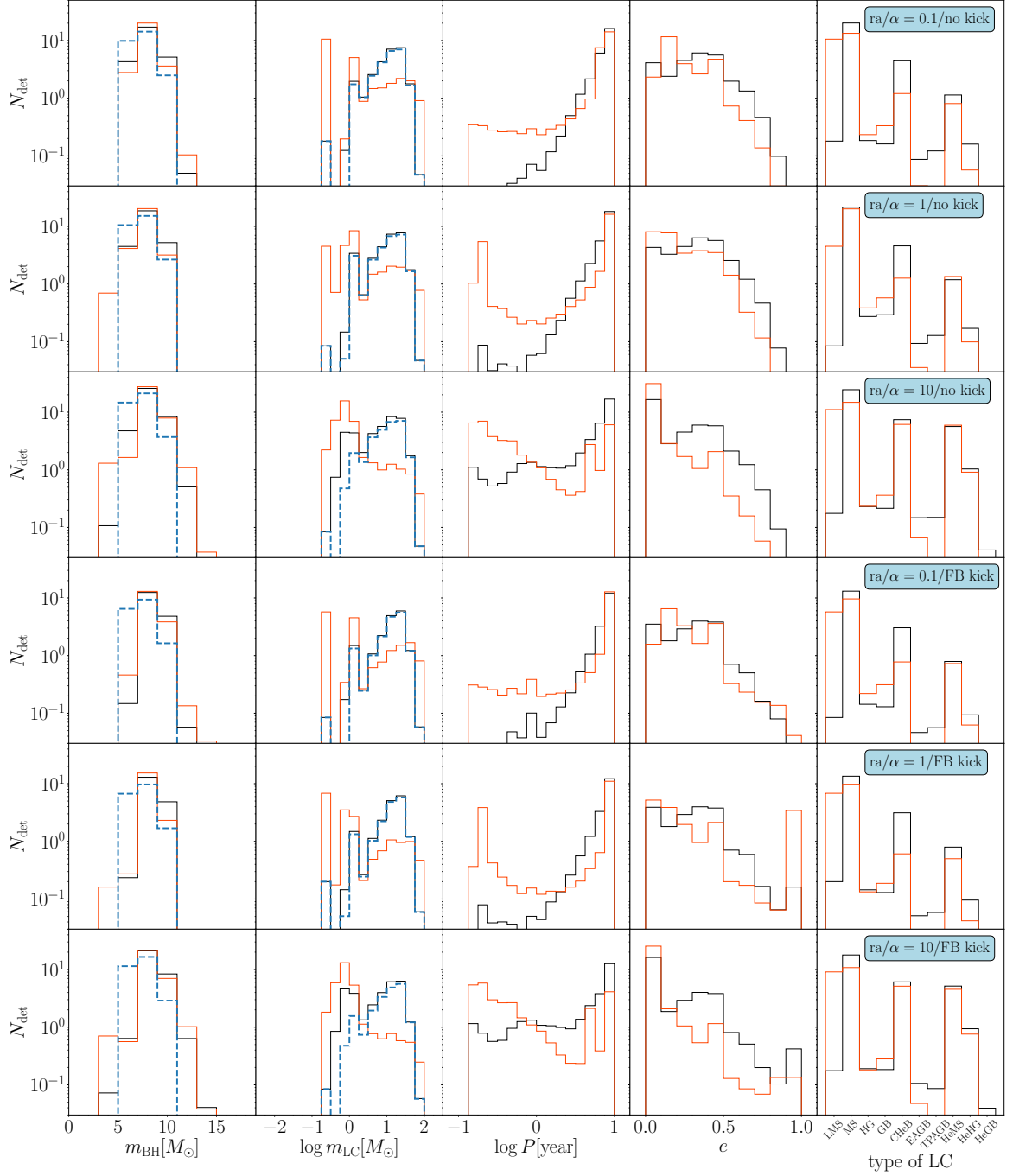


Figure 2. Binary parameter distributions of binaries formed with the rapid model. In each row from the top, the distributions of $\alpha = 0.1$ and no kick, $\alpha = 1$ and no kick, $\alpha = 10$ and no kick, $\alpha = 0.1$ and FB kick, $\alpha = 1$ and FB kick, and $\alpha = 10$ and FB kick models are shown. Starting on the left, there are BH mass, LC mass, orbital period, eccentricity, and LC type distributions. In LC type distribution, each abbreviation is following: “LMS”: low mass MS star ($m_{\text{LC}} \lesssim 0.7M_{\odot}$), “MS”: MS star ($m_{\text{LC}} \gtrsim 0.7M_{\odot}$), “HG”: Hertzsprung gap, “GB”: first giant branch, “CHeB”: core He burning, “EAGB”: first asymptotic giant branch, “TPAGB”: second asymptotic giant branch, “HeMS”: MS naked He star, “HeHG”: HG naked He star, and “HeGB”: GB naked He star. The black line is a distribution of detectable binaries and the red one shows the Galactic distribution of binaries with $P = 50$ days to 10 years normalized in N_{det} . In BH mass distribution, the blue dashed line corresponds to a distribution obtained from single star evolution. The blue dashed line in LC mass distribution shows a distribution of the detectable BH-LC binaries with LCs gaining their masses compared to the ZAMS stages.

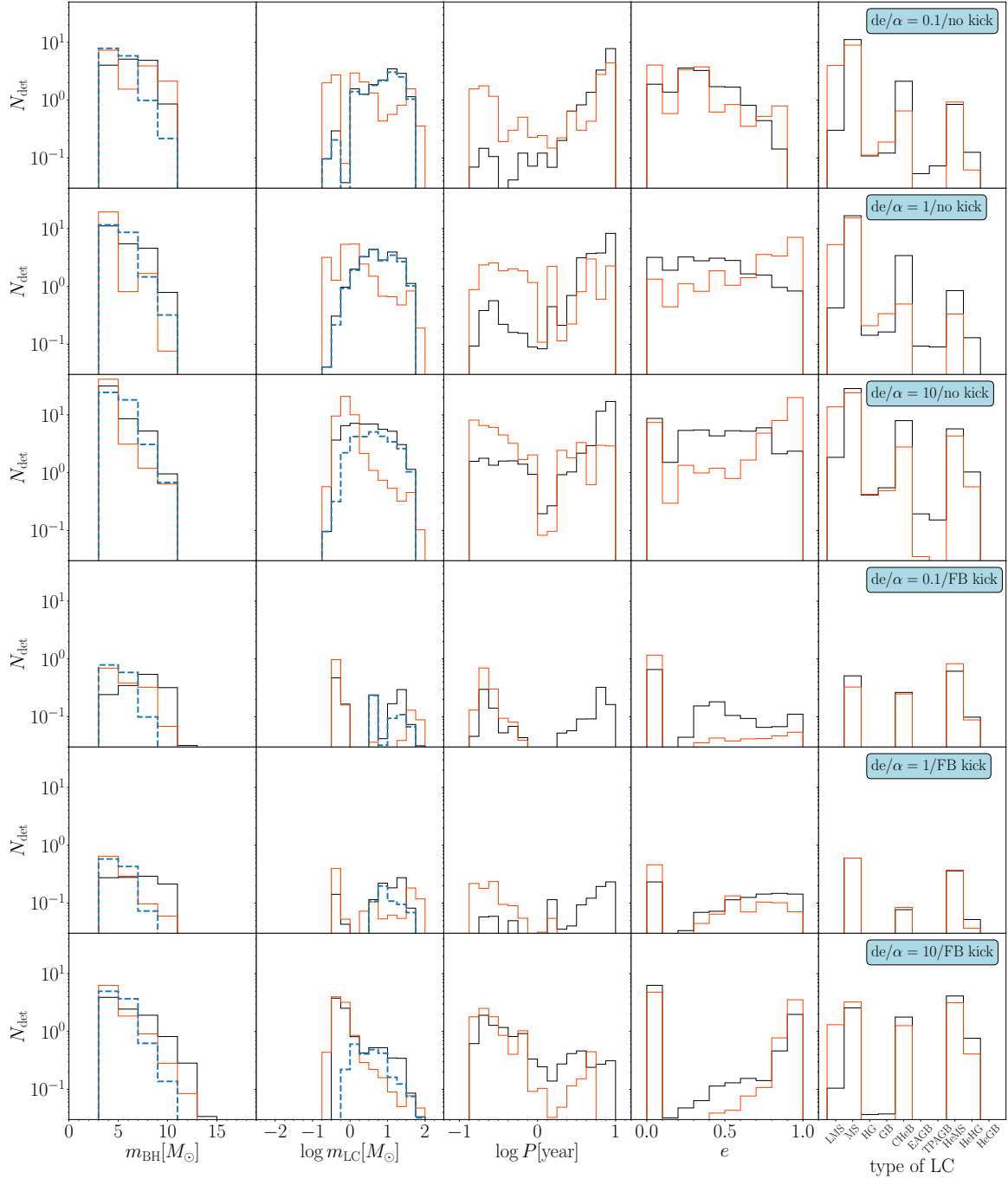


Figure 3. The same as Figure 2 except that SN model is the delayed model, not the rapid model.

Binary parameter distributions with each binary evolution model are shown in Figure 2 and 3. The red line in each panel shows the Galactic distribution of binaries with $P = 50$ days to 10 years, and the black line shows that of binaries detectable by *Gaia*. Note that for each line the total number of binaries is normalized to N_{det} . Except for the period distribution (the third panel from the left), though some small differences exist in each panel, the detectable binary distributions roughly reflect the features of the Galactic ones. The period distribution is biased to binaries with long period such as $P \gtrsim 1$ year compared to the Galactic distribution. That is because the observational constraint on the semi-major axis (equation 18) can be relaxed for looser binaries.

In the first panel from the left in Figure 2 and 3, BH mass distribution is shown. The blue dashed line depicts a mass distribution of BHs left behind after the death of a single star. The single stars follow the Kroupa’s IMF, and their evolution is calculated by the single star evolution (SSE) code (Hurley et al. 2000) which uses the same star evolution model as in BSE. The detectable distribution (black) as well as the Galactic (red) one and one obtained from SSE are very similar. This can be interpreted in the following way. In single stellar evolution, BH masses are determined by how much BH progenitors lose their masses through their stellar winds. In binary evolution, BH masses depend on not only strength of stellar winds but also binary interactions. Thus, BHs formed through binary evolution can have different masses from those through single stellar evolution. However, the effects of stellar winds are much larger than those of binary interactions, since stellar winds are strong due to the solar metallicity. This is why BH mass distributions are similar between the single and binary evolution.

From this result, the BH mass distribution (the first panel from the left) in the rapid model has a peak around $8M_{\odot}$, while, in the delayed model, a peak is around $\leq 5M_{\odot}$ and there is no gap structure. Therefore, if the lower mass gap is not intrinsic (*i.e.* the intrinsic BH mass distribution is consistent with the delayed model), *Gaia* will observe BHs with mass in that range. We will be able to identify the lower mass gap in BH mass as intrinsic or not from the observation.

In addition, for all the combinations of SN and natal kick models, as CE efficiency becomes high ($\alpha = 10$), high mass BHs ($m_{\text{BH}} \gtrsim 11M_{\odot}$) are formed and become more observable compared to low CE efficiency models. The high CE efficiency can make more binaries avoid mergers in CE phases, and evolve to tight (but detectable) BH-LC binaries. In such tight BH-LC binaries, the BHs accrete masses from their companions through mass transfer, and grow to such heavy BHs. Note that the BH growth rate is smaller than the Eddington mass accretion rate.

From LC mass distributions (the second panel from the left), the detectable distribution is slightly biased to heavy LCs. This trend is seen in all the models. This is because heavier LCs are more luminous and easier to detect. In addition, for both SN models with $\alpha = 10$, some light LCs ($m_{\text{LC}} \leq 0.3M_{\odot}$) become detectable compared to other CE efficiency models. This is because, thanks to the high efficiency, binaries with light LCs expel the envelope efficiently through CE phase and can survive as tight BH-LC binaries. Thus, a significant number of short period binaries with light LCs are formed and become detectable as seen in the third panels from left. Thus, when we observe short period binaries with light LCs, CE efficiency should be significantly large.

For all the models, the blue lines in LC mass distributions indicate that most of the detectable LCs gain their masses by binary interaction. Therefore, the LCs may retain some footprints of the BH progenitors and we expect that detailed observations of LCs can make it clear how the BH-LC binaries were formed. Such footprints were reported in low-mass X-ray binaries (LMXBs) accompanying BHs as chemical anomalies of LC companions (see Casares et al. 2017, for a review)(Israelian et al. 1999; Orosz et al. 2001; González Hernández et al. 2004, 2005, 2006, 2011). Although LCs in detectable BH binaries with *Gaia* may be less polluted than those in LMXBs because of their wider separations, detailed observations of LCs in BH binaries will be helpful to elucidate the origins of chemical anomalies of LCs in LMXBs.

For both kick models with the rapid model and no kick model with the delayed model, the detectable period distributions (the third panel from the left) are greatly biased to a large value. That is because the motion of LCs with large period binaries can be easily detected. However, for the delayed model with FB kick, a shape of the detectable period distribution varies with a choice of CE efficiency α . For $\alpha = 0.1$ case, two peaks are around 0.2 year and 5 year. Short period binaries evolve from initially loose and near-circular orbit binaries such as semi-major axis $a_{\text{ini}} \sim 10 - 600$ AU and eccentricity $e_{\text{ini}} \lesssim 0.5$ with heavy secondaries ($m_{\text{sec,ini}} \sim 8 - 20M_{\odot}$). Thanks to the inefficient CE efficiency, a significant number of binaries become very tight and survive after suffering FB kick, resulting in living long such as for tens of Myr. Thus, the first peak is seen in short period region. Though long period binaries are more likely to be disrupted by FB kick than short period ones and thus the number of long period binaries is small, they are easier to detect and the second peak can be seen in the long period region. For higher CE efficiency models ($\alpha = 1$ and 10), most of the tight binaries are disrupted because the high CE efficiencies prevent them from becoming tight enough to survive after suffering from FB kick. Thus, the short period peak disappears and the detectable distribution is biased to only longer period in $\alpha = 1$ case. However, a significant number of tight period binaries can be formed and become observable in $\alpha = 10$ case. They evolve from a different population from $\alpha = 0.1$ model, that is, initially tight and eccentric orbit binaries ($a_{\text{ini}} \sim 0.5 - 3$ AU and $e_{\text{ini}} \gtrsim 0.7$) with light secondaries ($m_{\text{sec,ini}} \sim 0.25 - 5M_{\odot}$). The initially high eccentricities can make these binaries enter CE phases, since the binary stars touch with each other

at their periapsises. If CE efficiency is not high (*i.e.* $\alpha = 1$), such binaries cannot expel the donors' envelopes and merge.

In the fourth left panels, we can see that the eccentricities of the detectable BH-LC binaries are slightly biased to a large value except for the delayed model with FB kick. The rapid model seems to be robust to FB kick because f_{fb} in the rapid model tends to be larger than that in the delayed model and they do not suffer from FB kick very much. When binaries experienced CE phase, the orbits become circularized and tighter, and the resulting BH-LC binaries are difficult to observe. Hence, the eccentricity distribution of detectable BHs is biased towards larger eccentricities. In particular, we found that eccentric long period binaries such as $P \sim 10$ years tend to preserve their initial eccentricities. However, for the delayed model, FB kick tends to disrupt eccentric binaries with long periods and tight binaries with circular orbits are likely to survive. Thus, the Galactic eccentricity distribution is biased to zero and we may be able to distinguish the existence of BH natal kick from the eccentricity distribution.

Finally, LC type distributions (the fifth panels from the left) tell us that the majority of detectable binaries have MS star companions except for the delayed model with FB kick. A significant number of BH-MS star (LC type 1), Core Helium burning (type 4) and MS He star (type 7) binaries have long lifetime such as ≥ 100 Myr, greatly contributing to N_{det} . For the delayed model with FB kick, the majority of such long lifetime binaries are disrupted by FB kick since they have light BHs $m_{\text{BH}} \lesssim 4M_{\odot}$ and greatly suffer from the kick. Thus, the LC type distribution is different from those of the other models.

According to BH mass distribution, our results also indicate that lower mass gap BH-LC binaries can be formed even in the rapid models, although the expected detectable number is less than unity. By mass accretion from secondaries, NSs gain their masses and evolve to low mass BHs with $m_{\text{BH}} \sim 3M_{\odot}$. We do not get high mass BHs with $\sim 20 M_{\odot}$ like Cygnus X-1 (Miller-Jones et al. 2021). This is because we take into account stronger stellar wind mass loss than inferred by the BH mass in Cygnus X-1.

3.2. The Effect of a Choice of P_{min} and P_{max} on the Detectability

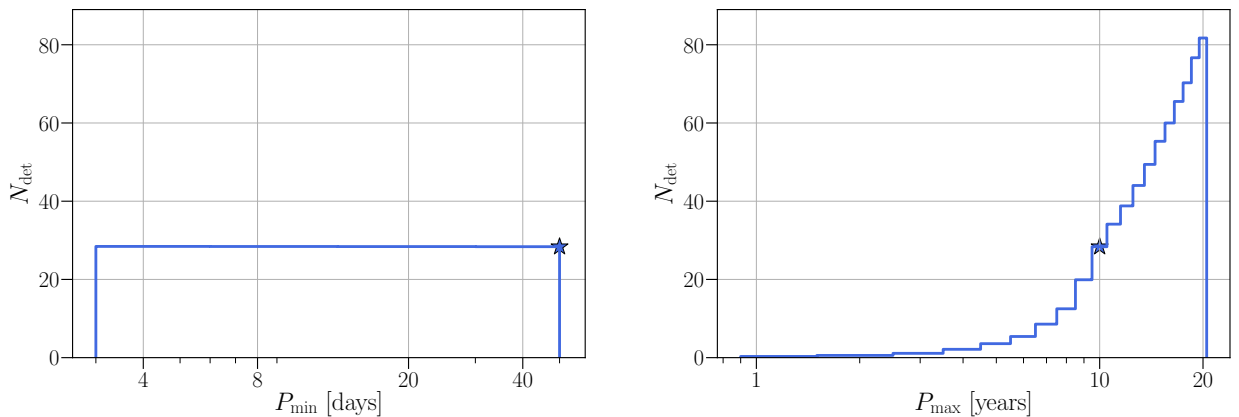


Figure 4. (Left) The relationship between a choice of the minimum period P_{min} and the detectability N_{det} of rapid/ $\alpha = 1$ /no kick model. (Right) The relationship between a choice of the maximum period P_{max} and the detectability N_{det} of rapid/ $\alpha = 1$ /no kick model. The star marker corresponds to P_{min} and P_{max} employed so far, e.g. $P_{\text{min}} = 50$ days or $P_{\text{max}} = 10$ years.

In addition to the binary evolution models, we investigate how choices of P_{min} and P_{max} affect the detectability in this section. BH-LC binaries with rapid/ $\alpha = 1$ /no kick model and a various values of the minimum period P_{min} , 4, 8, 20, and 40 days. The detectability of $P_{\text{min}} = 4$ days increases by at most 0.3 % compared with that of $P_{\text{min}} = 40$ days. This is *not* because the number of short-period BH-LC binaries is small. Rather, they are difficult to be detected, since their proper motions are small due to their short periods. The right panel in Figure 4 indicates how the detectability in rapid/ $\alpha = 1$ /no kick model will change when we choose a various value of P_{max} from 1 year to 20 years. In the calculations used for Figure 1 to 3, we adopted 10 years as P_{max} . If we extend it to 20 years, N_{det} will increase up to ~ 82 .

In Figure 5, the distributions of BH mass m_{BH} , LC mass m_{LC} and an orbital period P are shown. The distributions do not depend on P_{min} as compared between the black and blue lines, and between the red and green curves. This is because the number of the detectable BH-LC binaries does not increase even if P_{min} becomes smaller, as described

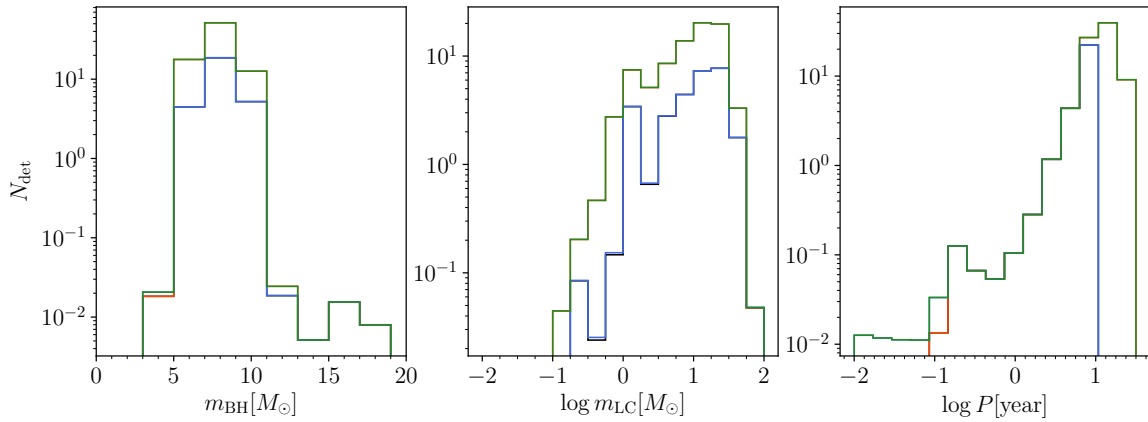


Figure 5. Binary parameter distributions of rapid/ $\alpha = 1$ /no kick model with a various pairs of P_{\min} and P_{\max} , 40 days and 10 years (black), 40 days and 20 years (red), 4 days and 10 years (blue), and 4 days and 20 years (green).

above. Although the number of detectable BH-LC binaries increases with P_{\max} increasing, the BH and LC mass distributions have similar shapes for different P_{\max} . In summary, the choices of P_{\min} and P_{\max} do not much affect the BH and LC mass distributions of detectable BH-LC binaries.

4. DISCUSSION

4.1. Comparisons with Previous Studies

Here, we compare the results with the previous work. Though Breivik et al. (2017) did not include some of the constraints we employed, we obtained similar results to those Breivik et al. (2017) obtained for the rapid model: FB kick does not affect both the detectability and the parameter distributions of detectable binaries very much. Shao & Li (2019) considered only interstellar extinction. Since we adopted two more observational constraints as well as the extinction, it is reasonable that our detectability is significantly smaller than they estimated.

Yamaguchi et al. (2018) and Yalinewich et al. (2018), which used the same constraints as ours, estimated more than 10 times larger number of BH-LC binaries can be detected. They also reported different LC mass distributions from ours. Yamaguchi et al. (2018) indicated LC mass distributions are biased to heavier values such as $\sim 10 - 20M_{\odot}$. Yalinewich et al. (2018) also suggested a double-peak distribution around $\sim 1M_{\odot}$ and $\sim 30M_{\odot}$. It is difficult to specify reasons for the difference between their and our results. They adopted analytic models, while we performed binary population synthesis calculations. There are many different points, such as single star evolution models, stellar winds, CE parameters, and tidal evolution models.

Chawla et al. (2021) employed both the rapid and the delayed models with including FB kick, similarly to us. They estimated the number of detectable BH-LC binaries larger than we estimated by 3–10 times. We conclude that our results would be similar to theirs, despite of different observational constraints adopted. They expected that *Gaia* observations could give a constraint on binary evolution models, such as SN models, which is consistent with our results. Moreover, our systematic study for binary evolution models shows that the CE efficiency α could be also constrained, and that the natal kick model could be identified if the delayed model is correct.

4.2. Model Uncertainties

In the eccentricity distribution, we found that for most of the parameter sets, the detectable BH distributions are biased to larger values. Here we discuss the above argument that eccentric and long-period BH-LC binaries tend to preserve their initial eccentricities, considering an uncertainty of tidal evolution in binaries. Yoon et al. (2010) (see also Qin et al. 2018) suggested another formula for dynamical tide, and Kinugawa et al. (2020) and Tanikawa et al. (2021) took into account it in their binary population synthesis to investigate formation of merging binary BHs. Tanikawa et al. (2021) found that their dynamical tide is less efficient than that in the original BSE for MS and post-MS stars, and more efficient for He stars. Since the majority of detectable BH-LC binaries have MS stars as LCs, eccentricities of long-period BH-LC binaries should be well preserved even if we employ the formula in Yoon et al. (2010). Thus, the above argument would not be sensitive to at least an uncertainty of tidal evolution in binaries.

In this work, we only consider the solar metallicity. If we include lower metallicity than the solar value (hereafter, the lower metallicity case), stars will not lose their masses compared to the solar metallicity case and lighter primary stars can form BHs. Thus, more BH-LC binaries will be formed and the detectability will increase. For BH mass distribution, more massive BHs such as $m_{\text{BH}} \geq 20M_{\odot}$ can be formed with both SN models, but the lower mass gap BHs can be formed only with the delayed model. Based on the important statement that the detectable BH mass distribution is similar to the Galactic one and the distribution obtained from SSE, *Gaia* will detect the lower mass gap BHs if SN model is consistent with the delayed model. The strength of FB kick should be weakened in the lower metallicity case and the effect of the kick might be somehow blurred. Although the dependence of BH-LC binary parameters on the CE efficiency α might be different between the solar and lower metallicity cases, the detailed discussion is beyond the scope of this work.

5. CONCLUSION

We simulated BH-LC binaries with a binary population synthesis code BSE and investigated how the detectability of BH-LC binaries with *Gaia* is affected by binary parameters such as SN models, CE efficiency, and natal kick. We employed two SN models, the rapid and the delayed models. The intrinsic BH mass gap is produced in the former model, and not in the latter model. We also adopted three different CE efficiency $\alpha = 0.1, 1, \text{ and } 10$ and checked the effect of natal kick by switching it on and off.

We estimated 1.1 – 46 BH-LC binaries can be observed in the five-year observation with *Gaia*. In each model, we found that parameter distributions of the detectable binaries are roughly consistent with the Galactic distributions. There are three important implications from our results:

1. from the BH mass distribution, if the lower mass gap is not intrinsic, *Gaia* will observe $\leq 5M_{\odot}$ BHs.
2. when we observe BH-LC binaries with short orbital periods and light LCs, a large CE efficiency should be favored.
3. while the rapid model is robust to FB kick, the delayed model is greatly affected by the kick. We may be able to distinguish the existence of the kick from the eccentricity distribution of detectable BH-LC binaries.

We also investigated whether choices of P_{min} and P_{max} will affect the detectability and the parameter distributions. With respect to the detectability and the parameter distributions, we found that the choice of P_{min} (*i.e.* the cadence of the astrometric observation) does not matter. By contrast, the choice of P_{max} can affect the detectability drastically. If we extend the maximum period up to 20 years from 10 years, we will find more than three times larger number of BH-LC binaries. If the *Gaia* operation is extended long enough and/or the method to identify BH-LC binaries from the *Gaia* data is more sophisticated, we can expect that we may find BH-LC binaries with orbital periods longer than 10 years.

ACKNOWLEDGEMENT

N.K. acknowledges support by the Hakubi project at Kyoto University. This research was supported in part by Grants-in-Aid for Scientific Research (17H06360, 19K03907) from the Japan Society for the Promotion of Science, and MEXT as “Program for Promoting Researches on the Supercomputer Fugaku” (towards a unified view of the universe: from large scale structures to planets, revealing the formation history of the universe with large-scale simulations and astronomical big data).

REFERENCES

- 1997, ESA Special Publication, Vol. 1200, The HIPPARCOS and TYCHO catalogues. Astrometric and photometric star catalogues derived from the ESA HIPPARCOS Space Astrometry Mission
- Abbott, B. P., Abbott, R., Abbott, T. D., et al. 2019, Phys. Rev. X, 9, 031040, doi: [10.1103/PhysRevX.9.031040](https://doi.org/10.1103/PhysRevX.9.031040)
- Abbott, R., Abbott, T. D., Abraham, S., et al. 2020, ApJL, 896, L44, doi: [10.3847/2041-8213/ab960f](https://doi.org/10.3847/2041-8213/ab960f)
- Agol, E., Kamionkowski, M., Koopmans, L. V. E., & Blandford, R. D. 2002, ApJL, 576, L131, doi: [10.1086/343758](https://doi.org/10.1086/343758)
- Andrews, J. J., Breivik, K., & Chatterjee, S. 2019, ApJ, 886, 68, doi: [10.3847/1538-4357/ab441f](https://doi.org/10.3847/1538-4357/ab441f)
- Bahcall, J. N., & Soneira, R. M. 1980, ApJS, 44, 73, doi: [10.1086/190685](https://doi.org/10.1086/190685)

- Belczynski, K., Bulik, T., Fryer, C. L., et al. 2010, *ApJ*, 714, 1217, doi: [10.1088/0004-637X/714/2/1217](https://doi.org/10.1088/0004-637X/714/2/1217)
- Bland-Hawthorn, J., & Gerhard, O. 2016, *Annual Review of Astronomy and Astrophysics*, 54, 529, doi: [10.1146/annurev-astro-081915-023441](https://doi.org/10.1146/annurev-astro-081915-023441)
- Breivik, K., Chatterjee, S., & Larson, S. L. 2017, *ApJL*, 850, L13, doi: [10.3847/2041-8213/aa97d5](https://doi.org/10.3847/2041-8213/aa97d5)
- Broekgaarden, F. S., & Berger, E. 2021, *ApJL*, 920, L13, doi: [10.3847/2041-8213/ac2832](https://doi.org/10.3847/2041-8213/ac2832)
- Brown, G. E., & Bethe, H. A. 1994, *ApJ*, 423, 659, doi: [10.1086/173844](https://doi.org/10.1086/173844)
- Casares, J., Jonker, P. G., & Israelian, G. 2017, *X-Ray Binaries*, ed. A. W. Alsabti & P. Murdin, 1499, doi: [10.1007/978-3-319-21846-5_111](https://doi.org/10.1007/978-3-319-21846-5_111)
- Chawla, C., Chatterjee, S., Breivik, K., et al. 2021, arXiv e-prints, arXiv:2110.05979. <https://arxiv.org/abs/2110.05979>
- Chu, Q., Yu, S., & Lu, Y. 2022, *MNRAS*, 509, 1557, doi: [10.1093/mnras/stab2882](https://doi.org/10.1093/mnras/stab2882)
- Claeys, J. S. W., Pols, O. R., Izzard, R. G., Vink, J., & Verbunt, F. W. M. 2014, *A&A*, 563, A83, doi: [10.1051/0004-6361/201322714](https://doi.org/10.1051/0004-6361/201322714)
- Corral-Santana, J. M., Casares, J., Muñoz-Darias, T., et al. 2016, *A&A*, 587, A61, doi: [10.1051/0004-6361/201527130](https://doi.org/10.1051/0004-6361/201527130)
- de Kool, M. 1990, *ApJ*, 358, 189, doi: [10.1086/168974](https://doi.org/10.1086/168974)
- de Vaucouleurs, G. 1959, *Handbuch der Physik*, 53, 311
- Dewi, J. D. M., & Tauris, T. M. 2000, *A&A*, 360, 1043. <https://arxiv.org/abs/astro-ph/0007034>
- El-Badry, K., & Quataert, E. 2020, *MNRAS*, L2, doi: [10.1093/mnras/slaa004](https://doi.org/10.1093/mnras/slaa004)
- Eldridge, J. J., Stanway, E. R., Breivik, K., et al. 2020, *MNRAS*, 495, 2786, doi: [10.1093/mnras/staa1324](https://doi.org/10.1093/mnras/staa1324)
- Farr, W. M., Sravan, N., Cantrell, A., et al. 2011, *ApJ*, 741, 103, doi: [10.1088/0004-637X/741/2/103](https://doi.org/10.1088/0004-637X/741/2/103)
- Fragos, T., Andrews, J. J., Ramirez-Ruiz, E., et al. 2019, *ApJL*, 883, L45, doi: [10.3847/2041-8213/ab40d1](https://doi.org/10.3847/2041-8213/ab40d1)
- Fryer, C. L., Belczynski, K., Wiktorowicz, G., et al. 2012, *ApJ*, 749, 91, doi: [10.1088/0004-637X/749/1/91](https://doi.org/10.1088/0004-637X/749/1/91)
- Gaia Collaboration, Prusti, T., de Bruijne, J. H. J., et al. 2016, *A&A*, 595, A1, doi: [10.1051/0004-6361/201629272](https://doi.org/10.1051/0004-6361/201629272)
- Giesers, B., Dreizler, S., Husser, T.-O., et al. 2018, *MNRAS*, 475, L15, doi: [10.1093/mnras/slx203](https://doi.org/10.1093/mnras/slx203)
- González Hernández, J. I., Casares, J., Rebolo, R., et al. 2011, *ApJ*, 738, 95, doi: [10.1088/0004-637X/738/1/95](https://doi.org/10.1088/0004-637X/738/1/95)
- González Hernández, J. I., Rebolo, R., Israelian, G., et al. 2005, *ApJ*, 630, 495, doi: [10.1086/430755](https://doi.org/10.1086/430755)
- . 2004, *ApJ*, 609, 988, doi: [10.1086/421102](https://doi.org/10.1086/421102)
- . 2006, *ApJL*, 644, L49, doi: [10.1086/505391](https://doi.org/10.1086/505391)
- Gould, A., & Salim, S. 2002, *ApJ*, 572, 944, doi: [10.1086/340435](https://doi.org/10.1086/340435)
- Heggie, D. C. 1975, *MNRAS*, 173, 729, doi: [10.1093/mnras/173.3.729](https://doi.org/10.1093/mnras/173.3.729)
- Hobbs, G., Lorimer, D. R., Lyne, A. G., & Kramer, M. 2005, *MNRAS*, 360, 974, doi: [10.1111/j.1365-2966.2005.09087.x](https://doi.org/10.1111/j.1365-2966.2005.09087.x)
- Hurley, J. R., Pols, O. R., & Tout, C. A. 2000, *Monthly Notices of the Royal Astronomical Society*, 315, 543, doi: [10.1046/j.1365-8711.2000.03426.x](https://doi.org/10.1046/j.1365-8711.2000.03426.x)
- Hurley, J. R., Tout, C. A., & Pols, O. R. 2002, *MNRAS*, 329, 897, doi: [10.1046/j.1365-8711.2002.05038.x](https://doi.org/10.1046/j.1365-8711.2002.05038.x)
- Irrgang, A., Geier, S., Kreuzer, S., Pelisoli, I., & Heber, U. 2020, *A&A*, 633, L5, doi: [10.1051/0004-6361/201937343](https://doi.org/10.1051/0004-6361/201937343)
- Israelian, G., Rebolo, R., Basri, G., Casares, J., & Martín, E. L. 1999, *Nature*, 401, 142, doi: [10.1038/43625](https://doi.org/10.1038/43625)
- Jayasinghe, T., Stanek, K. Z., Thompson, T. A., et al. 2021, *MNRAS*, 504, 2577, doi: [10.1093/mnras/stab907](https://doi.org/10.1093/mnras/stab907)
- Jordi, C., Gebran, M., Carrasco, J. M., et al. 2010, *A&A*, 523, A48, doi: [10.1051/0004-6361/201015441](https://doi.org/10.1051/0004-6361/201015441)
- Kiel, P. D., & Hurley, J. R. 2006, *MNRAS*, 369, 1152, doi: [10.1111/j.1365-2966.2006.10400.x](https://doi.org/10.1111/j.1365-2966.2006.10400.x)
- Kinugawa, T., Nakamura, T., & Nakano, H. 2020, *MNRAS*, 498, 3946, doi: [10.1093/mnras/staa2511](https://doi.org/10.1093/mnras/staa2511)
- Kinugawa, T., & Yamaguchi, M. S. 2018, arXiv e-prints, arXiv:1810.09721. <https://arxiv.org/abs/1810.09721>
- Kobulnicky, H. A., & Fryer, C. L. 2007, *ApJ*, 670, 747, doi: [10.1086/522073](https://doi.org/10.1086/522073)
- Kormendy, J. 1977, *ApJ*, 217, 406, doi: [10.1086/155589](https://doi.org/10.1086/155589)
- Kroupa, P. 2001, *Monthly Notices of the Royal Astronomical Society*, 322, 231, doi: [10.1046/j.1365-8711.2001.04022.x](https://doi.org/10.1046/j.1365-8711.2001.04022.x)
- Kuiper, G. P. 1935, *PASP*, 47, 15, doi: [10.1086/124531](https://doi.org/10.1086/124531)
- Liu, J., Zhang, H., Howard, A. W., et al. 2019, *Nature*, 575, 618, doi: [10.1038/s41586-019-1766-2](https://doi.org/10.1038/s41586-019-1766-2)
- Lucy, L. B. 2014, *A&A*, 563, A126, doi: [10.1051/0004-6361/201322649](https://doi.org/10.1051/0004-6361/201322649)
- Mapelli, M., & Giacobbo, N. 2018, *MNRAS*, 479, 4391, doi: [10.1093/mnras/sty1613](https://doi.org/10.1093/mnras/sty1613)
- Mashian, N., & Loeb, A. 2017, *MNRAS*, 470, 2611, doi: [10.1093/mnras/stx1410](https://doi.org/10.1093/mnras/stx1410)
- Miller-Jones, J. C. A., Bahramian, A., Orosz, J. A., et al. 2021, *Science*, 371, 1046, doi: [10.1126/science.abb3363](https://doi.org/10.1126/science.abb3363)
- O’Neil, K. K., Martinez, G. D., Hees, A., et al. 2019, *AJ*, 158, 4, doi: [10.3847/1538-3881/ab1d66](https://doi.org/10.3847/1538-3881/ab1d66)
- Orosz, J. A., Kuulkers, E., van der Klis, M., et al. 2001, *ApJ*, 555, 489, doi: [10.1086/321442](https://doi.org/10.1086/321442)
- O’Shaughnessy, R., Kim, C., Kalogera, V., & Belczynski, K. 2008, *ApJ*, 672, 479, doi: [10.1086/523620](https://doi.org/10.1086/523620)
- Özel, F., Psaltis, D., Narayan, R., & McClintock, J. E. 2010, *ApJ*, 725, 1918, doi: [10.1088/0004-637X/725/2/1918](https://doi.org/10.1088/0004-637X/725/2/1918)

- Podsiadlowski, P., Rappaport, S., & Han, Z. 2003, MNRAS, 341, 385, doi: [10.1046/j.1365-8711.2003.06464.x](https://doi.org/10.1046/j.1365-8711.2003.06464.x)
- Qin, Y., Fragos, T., Meynet, G., et al. 2018, A&A, 616, A28, doi: [10.1051/0004-6361/201832839](https://doi.org/10.1051/0004-6361/201832839)
- Safarzadeh, M., Ramirez-Ruiz, E., & Belczynski, K. 2019, arXiv e-prints, arXiv:1912.10456. <https://arxiv.org/abs/1912.10456>
- Samland, M. 1998, ApJ, 496, 155, doi: [10.1086/305368](https://doi.org/10.1086/305368)
- Shafter, A. W. 2017, ApJ, 834, 196, doi: [10.3847/1538-4357/834/2/196](https://doi.org/10.3847/1538-4357/834/2/196)
- Shao, Y., & Li, X.-D. 2019, ApJ, 885, 151, doi: [10.3847/1538-4357/ab4816](https://doi.org/10.3847/1538-4357/ab4816)
- Shapiro, S. L., & Teukolsky, S. A. 1983, Black holes, white dwarfs, and neutron stars : the physics of compact objects
- Shikauchi, M., Kumamoto, J., Tanikawa, A., & Fujii, M. S. 2020, PASJ, 72, 45, doi: [10.1093/pasj/psaa030](https://doi.org/10.1093/pasj/psaa030)
- Spitzer, L. 1978, Physical processes in the interstellar medium, doi: [10.1002/9783527617722](https://doi.org/10.1002/9783527617722)
- Tanikawa, A., Kinugawa, T., Kumamoto, J., & Fujii, M. S. 2020, PASJ, 72, 39, doi: [10.1093/pasj/psaa021](https://doi.org/10.1093/pasj/psaa021)
- Tanikawa, A., Yoshida, T., Kinugawa, T., et al. 2021, arXiv e-prints, arXiv:2110.10846. <https://arxiv.org/abs/2110.10846>
- Tetzlaff, N., Neuhäuser, R., & Hohle, M. M. 2011, MNRAS, 410, 190, doi: [10.1111/j.1365-2966.2010.17434.x](https://doi.org/10.1111/j.1365-2966.2010.17434.x)
- The LIGO Scientific Collaboration, the Virgo Collaboration, the KAGRA Collaboration, et al. 2021, arXiv e-prints, arXiv:2111.03606. <https://arxiv.org/abs/2111.03606>
- Thompson, T. A., Kochanek, C. S., Stanek, K. Z., et al. 2019, Science, 366, 637, doi: [10.1126/science.aau4005](https://doi.org/10.1126/science.aau4005)
- . 2020, Science, 368, eaba4356, doi: [10.1126/science.aba4356](https://doi.org/10.1126/science.aba4356)
- Torres, G. 2010, The Astronomical Journal, 140, 1158–1162, doi: [10.1088/0004-6256/140/5/1158](https://doi.org/10.1088/0004-6256/140/5/1158)
- van den Heuvel, E. P. J. 1992, Endpoints of stellar evolution: the incidence of stellar mass black holes in the Galaxy., Tech. rep.
- van den Heuvel, E. P. J., & Tauris, T. M. 2020, Science, 368, eaba3282, doi: [10.1126/science.aba3282](https://doi.org/10.1126/science.aba3282)
- Webbink, R. F. 1984, ApJ, 277, 355, doi: [10.1086/161701](https://doi.org/10.1086/161701)
- Yalinewich, A., Beniamini, P., Hotokezaka, K., & Zhu, W. 2018, MNRAS, 481, 930, doi: [10.1093/mnras/sty2327](https://doi.org/10.1093/mnras/sty2327)
- Yamaguchi, M. S., Kawanaka, N., Bulik, T., & Piran, T. 2018, ApJ, 861, 21, doi: [10.3847/1538-4357/aac5ec](https://doi.org/10.3847/1538-4357/aac5ec)
- Yoon, S.-C., Woosley, S. E., & Langer, N. 2010, The Astrophysical Journal, 725, 940, doi: [10.1088/0004-637x/725/1/940](https://doi.org/10.1088/0004-637x/725/1/940)
- Yungelson, L. R., & Lasota, J. P. 2008, A&A, 488, 257, doi: [10.1051/0004-6361:200809684](https://doi.org/10.1051/0004-6361:200809684)